doi: 10.18323/2782-4039-2025-1-71-2

Structure and mechanical properties of high-entropy alloys of the CoCrZrMnNi system with different Zr and Mn contents produced by vacuum-induction melting

Sergey V. Konovalov*[1,2,3], Doctor of Sciences (Engineering), Professor,
Vice-Rector for Research and Innovation Activities
Vladislav K. Drobyshev[1,4], postgraduate student of Chair of Metal Forming and Materials Science of EVRAZ ZSMK, researcher of the Laboratory of Electron Microscopy and Image Processing
Irina A. Panchenko[1,5], PhD (Engineering), assistant professor of Chair of Quality Management and Innovation, Head of the Laboratory of Electron Microscopy and Image Processing
Li Haixin[2,6], PhD, associate professor of Yantai Research Institute
[1]*Siberian State Industrial University, Novokuznetsk (Russia)*
[2]*Harbin Engineering University, Yantai (China)*

***E-mail:** konovalov@sibsiu.ru

[3]ORCID: https://orcid.org/0000-0003-4809-8660
[4]ORCID: https://orcid.org/0000-0002-1532-9226
[5]ORCID: https://orcid.org/0000-0002-1631-9644
[6]ORCID: https://orcid.org/0000-0002-3444-115X

Received 29.11.2024 *Revised 30.01.2025* *Accepted 19.02.2025*

Abstract: The mechanical properties and microstructure of high-entropy alloys (HEA) of the CoCrZrMnNi system produced by vacuum-induction melting are studied depending on the change in the Zr and Mn content. The effect of the Zr and Mn percentage on the microstructure and mechanical properties (Young's modulus, nanohardness, microhardness) of the high-entropy alloys of the CoCrZrMnNi system is estimated. The relationship between varying the percentage of Zr and Mn and changing the grain size and mechanical properties of high-entropy alloys is studied. The structure, chemical composition and distribution of the intensity of characteristic X-ray radiation of atoms are studied using scanning electron microscopy. The study by scanning electron microscopy methods has demonstrated that in CoCrZrMnNi alloys, with an increase in the zirconium content and a decrease in the manganese content closer to the equiatomic composition, the material structure became more homogeneous. Changing the percentage of zirconium from 8 to 28 at. % contributed to the grain size reduction from 30 to 5 μm and a more uniform elemental distribution. The $Co_{19.8}Cr_{17.5}Zr_{15.3}Mn_{27.7}Ni_{19.7}$ alloy demonstrated the highest nanohardness (10 GPa) and Young's modulus (161 GPa) during instrumental indentation with an indenter load of 50 mN. The $Co_{20.4}Cr_{18.0}Zr_{7.9}Mn_{33.3}Ni_{20.3}$ alloy has the lowest nanohardness, Young's modulus, and microhardness among other alloys, which may be related to the coarse-grained structure with a grain size of up to 30 μm. As the indenter load increased to 5 N, the microhardness of the $Co_{19.8}Cr_{17.5}Zr_{15.3}Mn_{27.7}Ni_{19.7}$ alloy decreased compared to the $Co_{18.7}Cr_{16.5}Zr_{28.9}Mn_{17.4}Ni_{18.6}$ alloy, which may indicate more universal mechanical properties of alloys with equiatomic zirconium content.

Keywords: structure; mechanical properties; high-entropy alloy; vacuum-induction melting; scanning electron microscopy; Young's modulus; nanohardness; microhardness.

Acknowledgments: The study was supported by the grant of the Russian Science Foundation No. 23-49-00015, https://rscf.ru/project/23-49-00015/.

For citation: Konovalov S.V., Drobyshev V.K., Panchenko I.A., Li Haixin. Structure and mechanical properties of high-entropy alloys of the CoCrZrMnNi system with different Zr and Mn contents produced by vacuum-induction melting. *Frontier Materials & Technologies*, 2025, no. 1, pp. 21–34. DOI: 10.18323/2782-4039-2025-1-71-2.

INTRODUCTION

A new class of metallic materials, high-entropy alloys (HEAs), possessing the necessary physical, mechanical and operational characteristics, are materials consisting of five or more elements in equal or similar concentrations [1–3]. An increase in the number of elements improves mutual solubility, facilitating the formation of a single-phase solid solution [4]. Some promising technological features of HEAs include high hardness [5], good wear resistance [6], excellent strength at both high and low temperatures [7; 8], and good resistance to oxidation and corrosion [9; 10]. The unique characteristics of these alloys are due to the intrinsic properties of a multicomponent solid solution, such as a distorted lattice structure [11], a cocktail effect [12], slow diffusion [5], and nanoscale twinning [9].

Among the HEAs, a comprehensively studied and promising material is the equiatomic CoCrFeMnNi composition called the Cantor alloy [13]. Although this material has a multicomponent chemical structure, it forms a single-phase solid solution with a face-centered cubic

lattice [14]. Due to this structure, the material demonstrates high plasticity at room temperature with a relative elongation before failure of ~71 %. However, the key disadvantage of the Cantor alloy remains the relatively low values of yield strength of ≈220 MPa and tensile strength of ≈491 MPa, which significantly narrows the area of their practical application [15]. In this regard, an urgent task in the development of the HEA of this system is to find methods for improving the strength characteristics without compromising on the reduction of plasticity.

In recent years, much work has been focused on the development of new HEA compositions with good mechanical characteristics [16]. A promising direction for improving the mechanical and functional properties of alloys is alloying with well-studied elements, for example, by adding zirconium [17]. Zirconium alloying has been studied to improve the mechanical properties of both light alloys [18] and steels [19], but the influence of zirconium on the mechanical properties of high-entropy Cantor alloys with Zr content up to 30 at. % has not yet been studied. The expected strengthening mechanism associated with Zr modifications in HEA is pinning of dislocations, which can be caused by a strong lattice distortion. This distortion, in turn, can be caused by substitution defects, vacancies, or phase mismatch [20]. Based on the study of the CoCrFeNiZr system alloy, the work [17] discusses the effect of zirconium on changes in the alloy microstructure, but does not investigate the dependence of changes in mechanical properties and structure with an increase in the zirconium content with a simultaneous decrease in the content of another component.

In this study, the authors study three compositions of high-entropy alloys of the CoCrZrMnNi system with a change in the concentration of zirconium and manganese in the alloy from ≈5 to ≈30 at. %.

The aim of this research is a detailed study of the microstructure and homogeneity of the distribution of elements in the produced alloys depending on the increase in the Zr content with a simultaneous decrease in Mn; analysis of the effect of zirconium additives on the change in microhardness, nanohardness, and Young's modulus of CoCrZrMnNi alloys; and selection of a composition with optimal mechanical properties.

METHODS

In this work, the authors investigated as-cast high-entropy CoCrZrMnNi system alloys with different zirconium and manganese contents (Table 1) produced by vacuum-induction melting.

Samples were cut from the produced ingots on a DK7732 M11 jet-type electrical discharge machine. To obtain a high-quality microsection surface for research, during grinding the authors successively moved from one sandpaper to another with continuously decreasing sizes of abrasive particles and then polished the sample using a special cloth and paste. To identify the microstructure of the samples, etching in a reagent consisting of HNO_3 and HCl in a ratio of 1:3 was carried out; the etching time was 10–30 s.

The structure and elemental composition of the samples were studied using scanning electron microscopy (SEM) (KYKY EM-6900 device (China) equipped with an Oxford Xplore energy-dispersive analyzer (UK)) with an accelerating voltage of 30 kV, a filament current of 2.20 A, and an emission current of $150 \cdot 10^{-6}$ A. The distribution of the intensity of the characteristic X-ray radiation of atoms was obtained by scanning along the line using X-ray microanalysis to determine the concentration heterogeneity of the alloys. This analysis was carried out on etched areas ranging from 80 to 600 μm in length.

The microhardness study was carried out using an HVS-1000A microhardness tester. The load was constant for all processing modes and was 5 N. The nanohardness and elastic modulus were measured using a NanoScan-4D nanohardness tester. The measurement method is indenting a diamond pyramid (indenter) with recording the force and depth of loading and subsequent calculation of hardness and modulus of elasticity in accordance with GOST 8.748-2011 (ISO 14577). Measurement procedure parameters: indenter is a triangular Berkovich pyramid; loading time is 10 s; unloading time is 10 s; maximum load maintenance time is 10 s; applied load is 50 mN.

RESULTS

The microstructure of the as-cast $Co_{19.8}Cr_{17.5}Zr_{15.3}Mn_{27.7}Ni_{19.7}$ high-entropy alloy produced by vacuum-induction remelting is shown in Fig. 1 and demonstrates a dendritic structure. The distribution of Co, Cr, Zr, Mn, and Ni was identified by mapping techniques. According to the data of conducted X-ray microanalysis, the content of elements presented in Table 2 was identified in the interdendritic (Fig. 1, spectra 1, 2) and dendritic regions (Fig. 1, spectra 3, 4) of the $Co_{19.8}Cr_{17.5}Zr_{15.3}Mn_{27.7}Ni_{19.7}$ alloy. The dendritic region is enriched in chromium and manganese, reaching 42 and 29 at. %, respectively, but is depleted in zirconium (≈1 at. %). The grain size of the chromium-enriched dendritic "islands" was 30 μm. Based on the distribution of the intensity of characteristic X-ray radiation of atoms shown in Fig. 2, one can conclude that the distribution of chromium, manganese and zirconium atoms is non-uniform.

In the alloy with a Zr content of 7.9 % and Mn content of 33.3 %, a quasi-uniform distribution of manganese, cobalt and nickel was identified (Fig. 3). The rest Zr and Cr elements demonstrate large-scale non-uniformities. The dendrites consist of an equimolar solid solution of Mn, Cr, Ni (Fig. 3, spectra 2–4), with the absolute amount of each component slightly higher than the nominal. Zirconium is mainly concentrated in the interdendritic regions (Fig. 3, spectrum 1, Table 3); these regions are also enriched in Ni and depleted in Cr. The interdendritic phase of the Zr-free alloy contains grains consisting of Mn and Cr. Based on the graph (Fig. 4), one can conclude that two compounds are formed in the 16–36 μm and 56–68 μm regions. In these regions, the concentration of manganese and nickel varies from 6 to 46 at. %.

Table 1. *Chemical composition of the studied samples of as-cast high-entropy alloys based on the CoCrZrMnNi system produced by the method of vacuum-induction melting*
Таблица 1. *Химический состав исследуемых образцов высокоэнтропийных сплавов в литом состоянии на основе системы CoCrZrMnNi, полученных методом вакуумной индукционной плавки*

Co, at. %	Cr, at. %	Zr, at. %	Mn, at. %	Ni, at. %
19.8	17.5	15.3	27.7	19.7
20.4	18.0	7.9	33.3	20.3
18.7	16.5	28.9	17.4	18.6

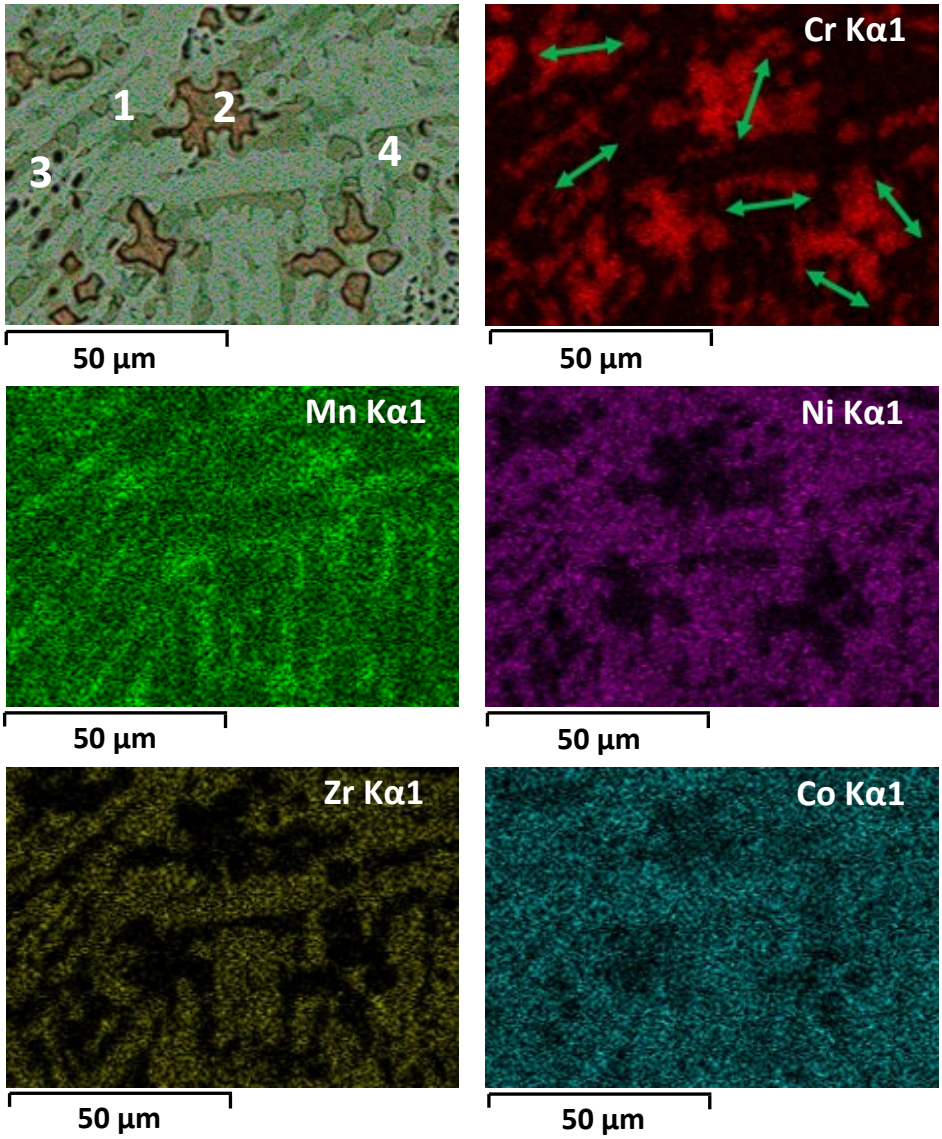

Fig. 1. *Elemental mapping of the $Co_{19.8}Cr_{17.5}Zr_{15.3}Mn_{27.7}Ni_{19.7}$ alloy.*
1–4 are sections of X-ray spectral microscanning. The arrows indicate the areas of dendrites measured in diameter
Рис. 1. *Элементное картирование сплава $Co_{19,8}Cr_{17,5}Zr_{15,3}Mn_{27,7}Ni_{19,7}$.*
1–4 – участки микрорентгеноспектрального сканирования.
Стрелками показаны области замеряемых дендритов по диаметру

Table 2. *The results of X-ray spectral microanalysis of the HEA presented in Fig. 1*
Таблица 2. *Результаты микрорентгеноспектрального анализа ВЭС по спектрам, представленного на рис. 1*

Spectrum	Element, at. %					
	Cr	Mn	Zr	Co	Ni	O
1	10.27	25.29	16.26	25.43	22.75	–
2	39.21	26.94	0.92	15.83	9.64	7.45
3	42.33	29.06	1.00	17.16	10.44	–
4	33.63	29.45	4.08	18.96	13.88	–

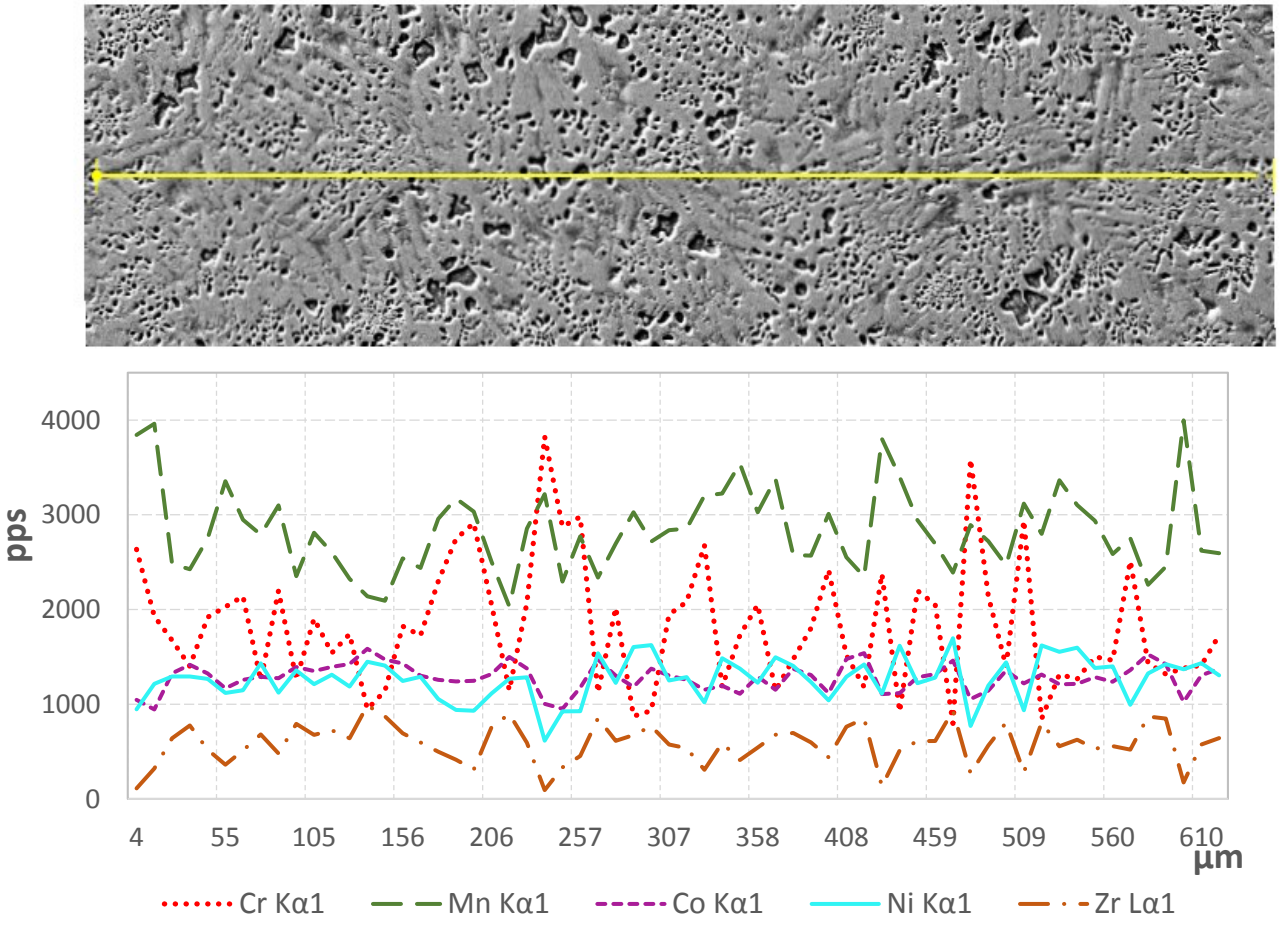

Fig. 2. *Analysis of concentration heterogeneity of the $Co_{19.8}Cr_{17.5}Zr_{15.3}Mn_{27.7}Ni_{19.7}$ alloy a line length of 600 µm*
Рис. 2. *Анализ концентрационной неоднородности сплава $Co_{19,8}Cr_{17,5}Zr_{15,3}Mn_{27,7}Ni_{19,7}$ вдоль линии протяженностью 600 мкм*

Analysis of the images obtained using SEM demonstrates the presence of elongated grains in the microstructure of the alloy (Fig. 5, spectrum 1). Despite the fact that the resulting high-entropy alloy has a non-equiatomic ratio of elements, among which Zr is predominant (Fig. 5, spectrum 1), its content in different regions decreases to 3 at. % (Fig. 5, spectrum 2) simultaneously with an increase in the content of Mn (30 at. %) and Ni (32 at. %). Elemental mapping demonstrated a uniform distribution of nickel, manganese, and cobalt (Fig. 5, spectrum 3). The microstructure analysis performed using SEM and a built-in EDS detector confirmed the non-uniform distribution of zirconium and chromium (Table 4), as well as the formation of globular inclusions containing Zr (Fig. 5).

Based on the distribution of the intensity of characteristic X-ray radiation of atoms shown in Fig. 6, it is possible to conclude about the non-uniform distribution of chromium, manganese and zirconium atoms. The size of

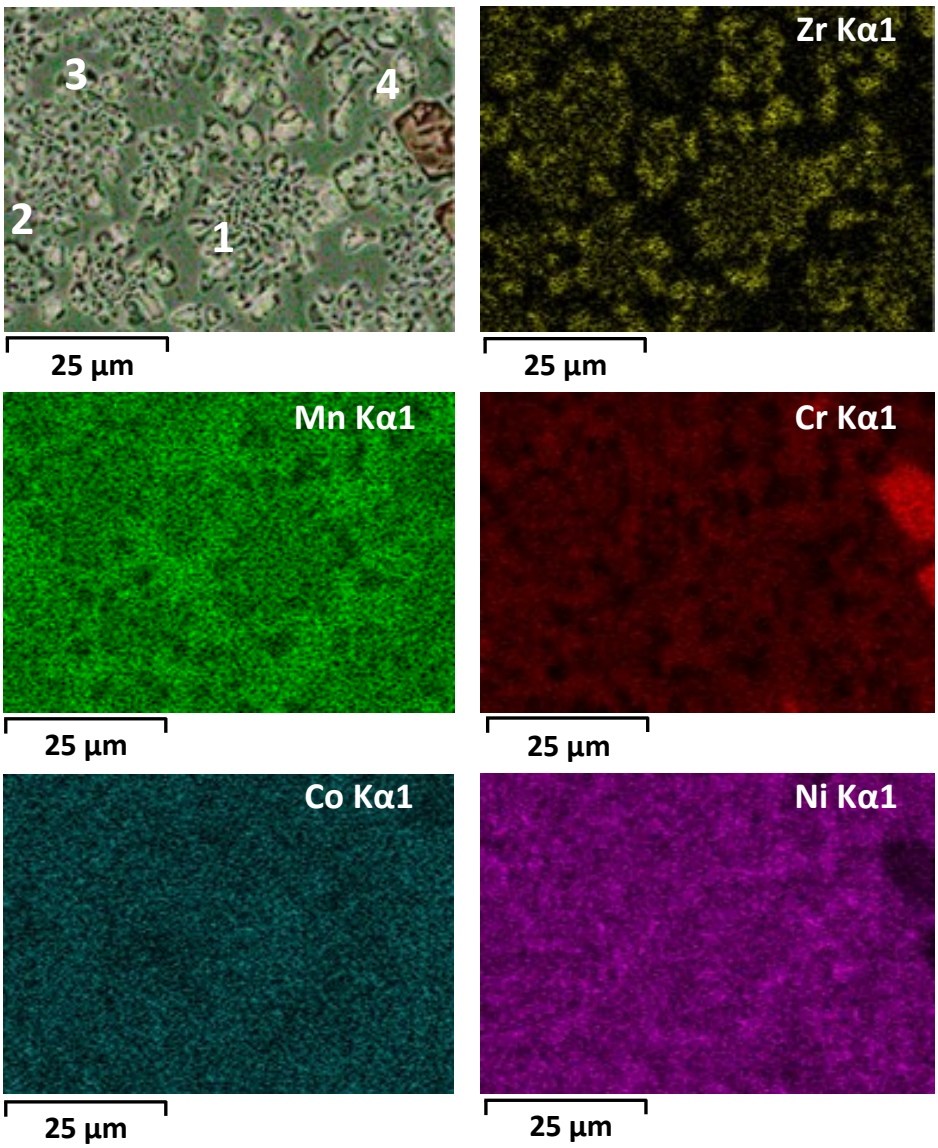

Fig. 3. *Elemental mapping of the $Co_{20.4}Cr_{18.0}Zr_{7.9}Mn_{33.3}Ni_{20.3}$ alloy. 1–4 are sections of X-ray spectral microscanning*
Рис. 3. *Элементное картирование сплава $Co_{20,4}Cr_{18,0}Zr_{7,9}Mn_{33,3}Ni_{20,3}$. 1–4 – участки микрорентгеноспектрального сканирования*

Table 3. *The results of X-ray spectral microanalysis of the HEA presented in Fig. 3*
Таблица 3. *Результаты микрорентгеноспектрального анализа ВЭС по спектрам, представленного на рис. 3*

Spectrum	Element, at. %				
	Cr	Mn	Zr	Co	Ni
1	5.98	26.24	14.00	20.65	33.14
2	45.92	21.78	1.00	21.75	10.55
3	16.33	40.62	1.46	17.69	23.91
4	45.92	21.78	1.00	21.75	10.55

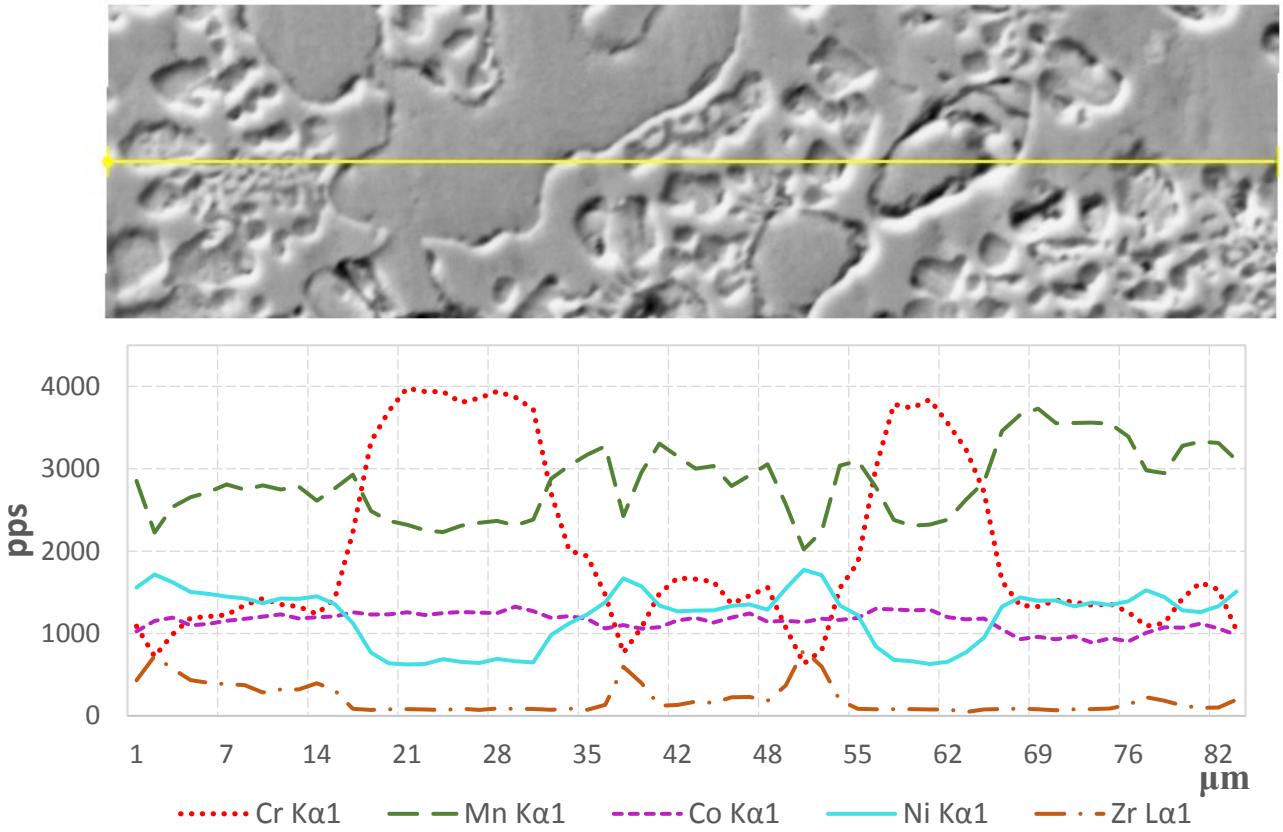

Fig. 4. *Determination of concentration heterogeneity of the* $Co_{20.4}Cr_{18.0}Zr_{7.9}Mn_{33.3}Ni_{20.3}$ *alloy a line length of 90 µm*
Рис. 4. *Определение концентрационной неоднородности сплава* $Co_{20,4}Cr_{18,0}Zr_{7,9}Mn_{33,3}Ni_{20,3}$ *вдоль линии протяженностью 90 мкм*

Table 4. *The results of X-ray spectral microanalysis of the HEA presented in Fig. 5*
Таблица 4. *Результаты микрорентгеноспектрального анализа ВЭС по спектрам, представленного на рис. 5*

Spectrum	Element, at. %				
	Cr	Mn	Zr	Co	Ni
1	18.31	16.27	24.26	23.21	17.95
2	10.74	30.21	3.87	23.18	32.00
3	12.76	22.28	19.65	20.98	24.32

the areas of non-uniform distribution of elements is up to 10 µm (Fig. 6).

The change in nanohardness and microhardness in CoCrZrMnNi alloys with an increase in the zirconium content and a decrease in the manganese content is distributed non-linearly. Thus, in the $Co_{19.8}Cr_{17.5}Zr_{15.3}Mn_{27.7}Ni_{19.7}$ alloy, the nanohardness values obtained in the interdendritic phase enriched with zirconium were 11 GPa, which is higher compared to the measurements carried out in the dendritic region equal to 9 GPa. These nanohardness values are the best among the other alloys studied. With an increase in the indenter load from 50 mN to 5 N, the microhardness of the $Co_{19.8}Cr_{17.5}Zr_{15.3}Mn_{27.7}Ni_{19.7}$ alloy decreases compared to the $Co_{18.7}Cr_{16.5}Zr_{28.9}Mn_{17.4}Ni_{18.6}$ alloy by 10 %. In general, the trend of increasing zirconium content has a positive effect on the increase in the microhardness of the material changing from 295 to 553 $HV_{0.5}$ (Fig. 7, Table 5). Thus, the alloy with the element content close to equimolar $Co_{18.7}Cr_{16.5}Zr_{28.9}Mn_{17.4}Ni_{18.6}$ alloy demonstrates better hardening ability compared to alloys with a nominal zirconium content of 7 and 15 %. Mechanically (elastic modulus), the $Co_{20.4}Cr_{18.0}Zr_{7.9}Mn_{33.3}Ni_{20.3}$ and $Co_{18.7}Cr_{16.5}Zr_{28.9}Mn_{17.4}Ni_{18.6}$

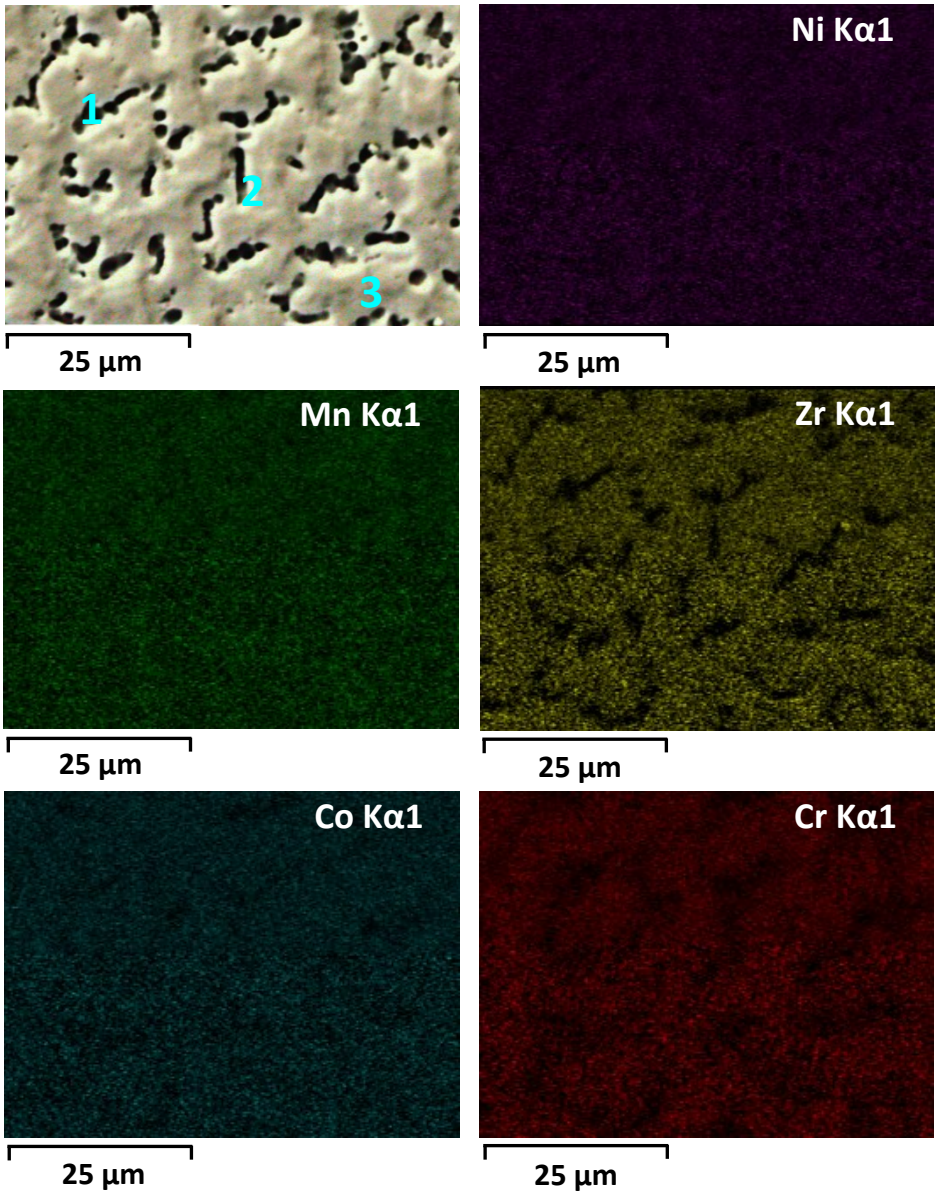

Fig. 5. *Elemental mapping of the* $Co_{18.7}Cr_{16.5}Zr_{28.9}Mn_{17.4}Ni_{18.6}$ *alloy. 1–3 are sections of X-ray spectral microscanning*
Рис. 5. *Элементное картирование сплава* $Co_{18,7}Cr_{16,5}Zr_{28,9}Mn_{17,4}Ni_{18,6}$. *1–3 – участки микрорентгеноспектрального сканирования*

alloys differ little, demonstrating very similar values – 122.73±10.37 and 109±10.41 GPa, respectively.

The microstructure of the as-cast CoCrZrMnNi alloy with nonequimolar Zr (8 at. %) and Mn (33 at. %) contents (Fig. 8 c, 8 d) consists predominantly of large dendrites with an increased chromium content of up to 46 % (Table 3). An increase in the zirconium content in the interdendritic regions of the $Co_{20.4}Cr_{18.0}Zr_{7.9}Mn_{33.3}Ni_{20.3}$ alloy reached 14 at. %. With an increase in the Zr content and a decrease in the Mn content closer to the equiatomic composition, the structure of the material became more uniform and the grain size decreased from 30 (Fig. 8 a, 8 b) to 5 µm (Fig. 8 e, 8 f). The smallest dendritic grains are found in the $Co_{18.7}Cr_{16.5}Zr_{28.9}Mn_{17.4}Ni_{18.6}$ alloy, located from the edge of the sample to the center.

DISCUSSION

In Fig. 1, the interdendritic phase of the Zr-free alloy contains small spherical inclusions (10 µm in diameter) consisting of Mn and Cr oxides. The formation of such inclusions has been previously noted by several authors. Apparently, inclusions are difficult to avoid when producing materials melted in a vacuum-induction furnace [21]. The reason for their presence is partial oxidation of the charge material, as evidenced by the data in Table 2 obtained by the X-ray microanalysis method.

Probably, the alignment of dendritic grains is associated with the direction of heat flow during solidification. In all the studied alloys, a quasi-homogeneous distribution of cobalt atoms was noted in elemental mapping (Figs. 1, 3, 5), thereby the percentage content of cobalt corresponds to

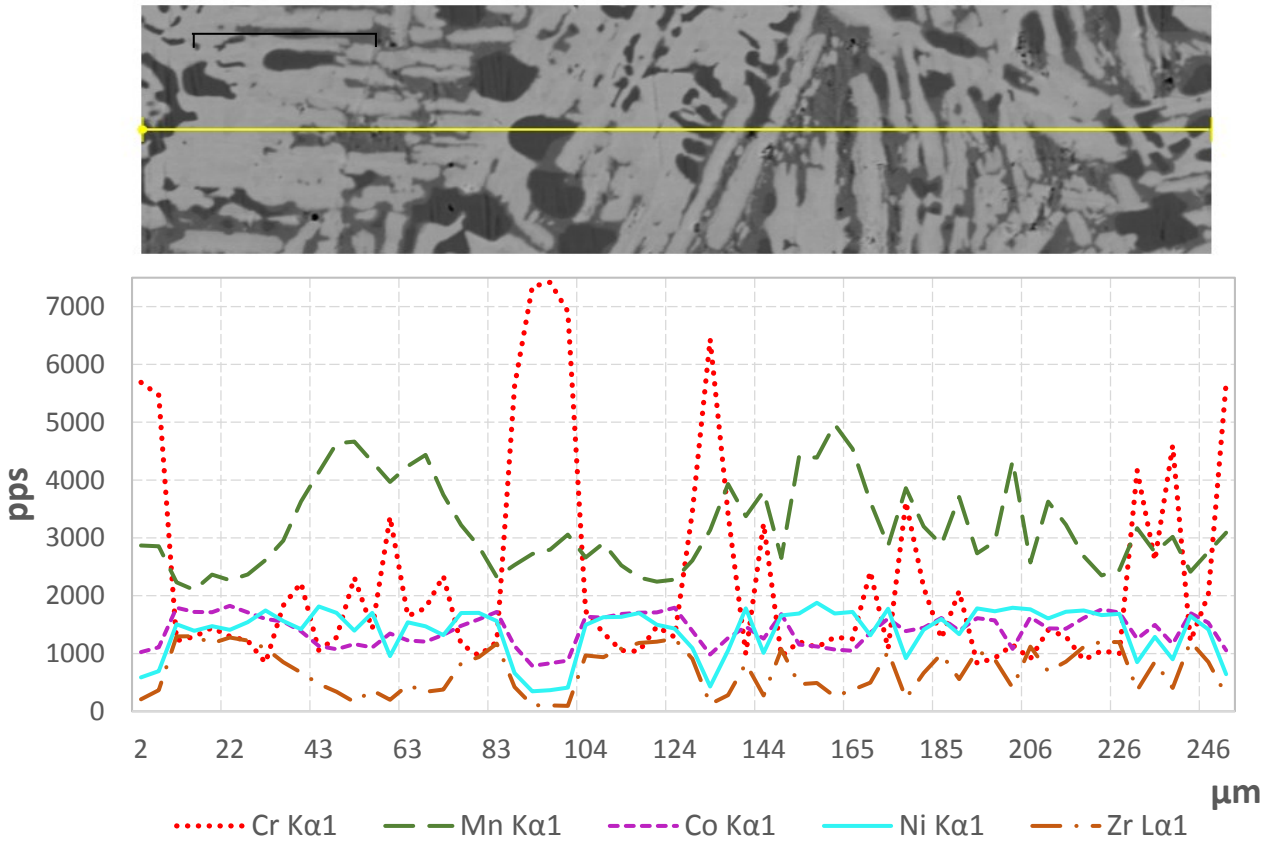

Fig. 6. *Determination of concentration heterogeneity of the $Co_{18.7}Cr_{16.5}Zr_{28.9}Mn_{17.4}Ni_{18.6}$ alloy along a line length of 246 µm*
Рис. 6. *Определение концентрационной неоднородности сплава $Co_{18,7}Cr_{16,5}Zr_{28,9}Mn_{17,4}Ni_{18,6}$ вдоль линии протяженностью 246 мкм*

Table 5. *Changes in the mechanical properties of CoCrZrMnNi alloys depending on changes in the zirconium and manganese content*
Таблица 5. *Изменение механических свойств сплавов CoCrZrMnNi в зависимости от изменения содержания циркония и марганца*

Average value			
Indenter penetration depth, nm	**Nanohardness, GPa**	**Young's modulus, GPa**	**Microhardness, HV0.5**
$Co_{19.8}Cr_{17.5}Zr_{15.3}Mn_{27.7}Ni_{19.7}$			
425.41±0.28	10.05±1.03	161.67±20.57	484±58
$Co_{20.4}Cr_{18.0}Zr_{7.9}Mn_{33.3}Ni_{20.3}$			
745.22±43.63	3.48±0.38	122.73±10.37	334±35
$Co_{18.7}Cr_{16.5}Zr_{28.9}Mn_{17.4}Ni_{18.6}$			
454.30±23.45	8.95±0.83	109.96±10.41	537±57

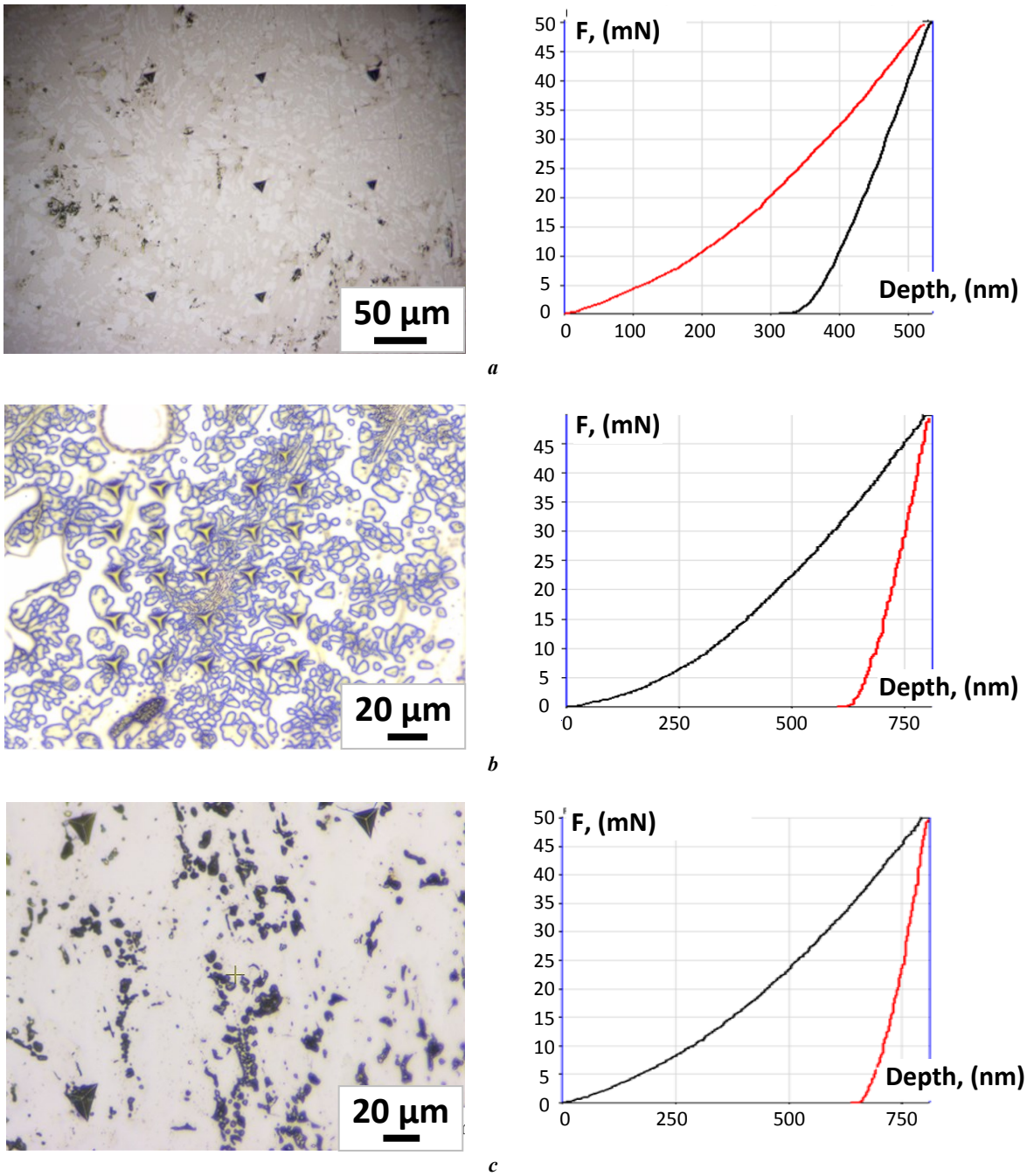

Fig. 7. *Optical image and loading–unloading graph of instrumental indentation of CoCrZrMnNi alloys:* ***a*** *–* $Co_{19,8}Cr_{17,5}Zr_{15,3}Mn_{27,7}Ni_{19,7}$; ***b*** *–* $Co_{20,4}Cr_{18,0}Zr_{7,9}Mn_{33,3}Ni_{20,3}$; ***c*** *–* $Co_{18,7}Cr_{16,5}Zr_{28,9}Mn_{17,4}Ni_{18,6}$

Рис. 7. *Оптическое изображение и график разгружения – нагружения инструментального индентирования сплавов CoCrZrMnNi:* ***a*** *–* $Co_{19,8}Cr_{17,5}Zr_{15,3}Mn_{27,7}Ni_{19,7}$; ***b*** *–* $Co_{20,4}Cr_{18,0}Zr_{7,9}Mn_{33,3}Ni_{20,3}$; ***c*** *–* $Co_{18,7}Cr_{16,5}Zr_{28,9}Mn_{17,4}Ni_{18,6}$

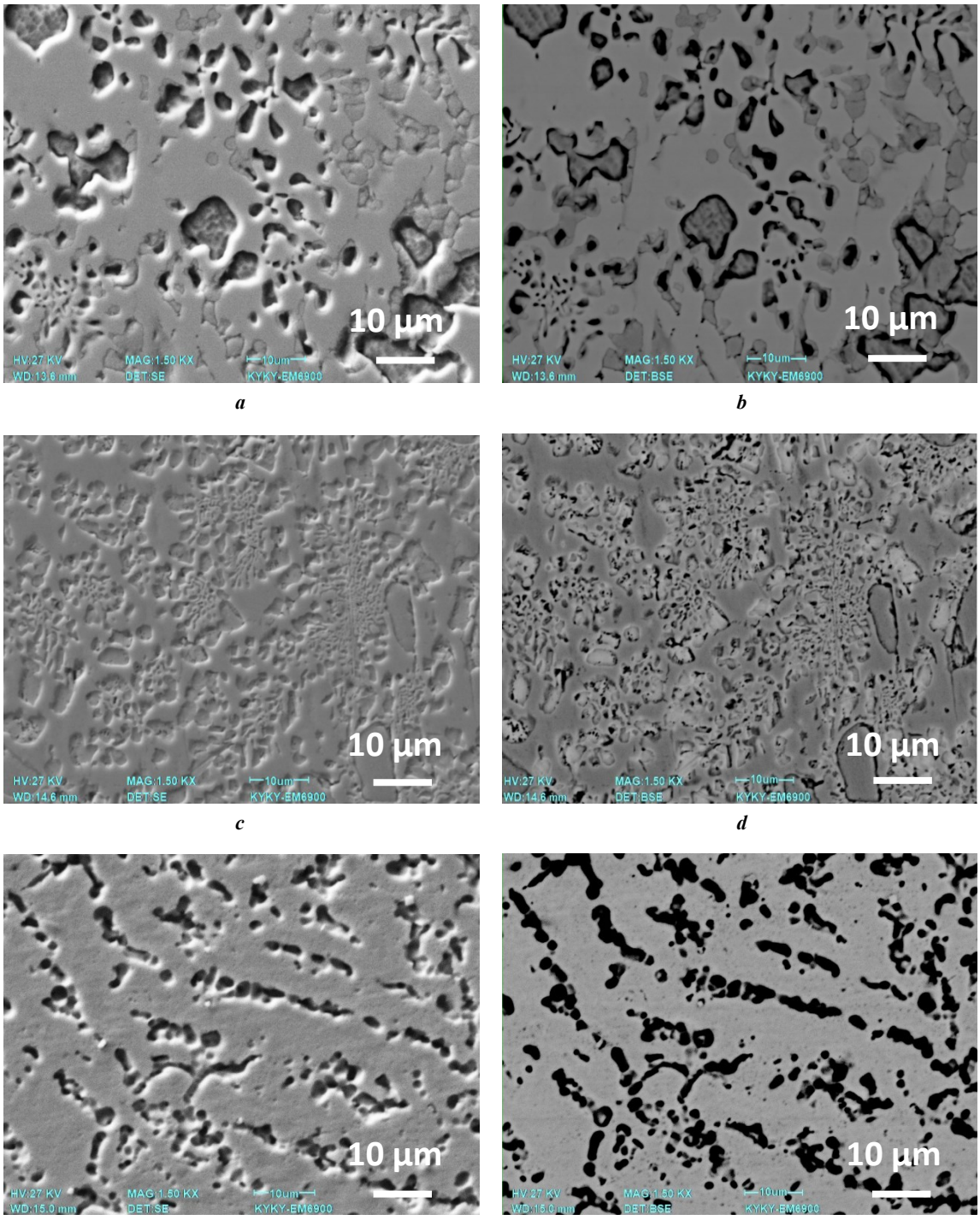

a *b*

c *d*

e *f*

Fig. 8. *Microstructure of CoCrZrMnNi alloys with different zirconium and manganese contents:*
a, b *– SEM of the* $Co_{19.8}Cr_{17.5}Zr_{15.3}Mn_{27.7}Ni_{19.7}$ *alloy using SE and BSE detector;*
c, d *– SEM of the* $Co_{20.4}Cr_{18.0}Zr_{7.9}Mn_{33.3}Ni_{20.3}$ *alloy using SE and BSE detector;*
e, f *– SEM of the* $Co_{18.7}Cr_{16.5}Zr_{28.9}Mn_{17.4}Ni_{18.6}$ *alloy using SE and BSE detector*
Рис. 8. *Микроструктура сплавов CoCrZrMnNi с разным содержанием циркония и марганца:*
a, b *– СЭМ сплава* $Co_{19,8}Cr_{17,5}Zr_{15,3}Mn_{27,7}Ni_{19,7}$ *с использованием SE и BSE детектора;*
c, d *– СЭМ сплава* $Co_{20,4}Cr_{18,0}Zr_{7,9}Mn_{33,3}Ni_{20,3}$ *с использованием SE и BSE детектора;*
e, f *– СЭМ сплава* $Co_{18,7}Cr_{16,5}Zr_{28,9}Mn_{17,4}Ni_{18,6}$ *с использованием SE и BSE детектора*

the nominal one in the studied alloys, which is consistent with the data of [22].

It is worth noting that the microhardness of the non-equiatomic $Co_{18.7}Cr_{16.5}Zr_{28.9}Mn_{17.4}Ni_{18.6}$ alloy (537±57 $HV_{0.5}$) (Table 5) exceeds the value for the $Co_{19.8}Cr_{17.5}Zr_{15.3}Mn_{27.7}Ni_{19.7}$ composition close to equiatomic (484±58 $HV_{0.5}$) [29], and the lowest values are observed in the alloy with a Zr content of 7.9 at. % and a Mn content of 33.3 at. %. This may be due to a finer grain structure reaching a size of about 5 μm and a more uniform distribution of elements in the $Co_{18.7}Cr_{16.5}Zr_{28.9}Mn_{17.4}Ni_{18.6}$ alloy compared to the $Co_{19.8}Cr_{17.5}Zr_{15.3}Mn_{27.7}Ni_{19.7}$ и $Co_{20.4}Cr_{18.0}Zr_{7.9}Mn_{33.3}Ni_{20.3}$ alloys. A similar pattern of changes in mechanical properties at nonequiatomic concentrations of Fe and Mn leading to an increase in the micro- and nanohardness of CoCrFeMnNi alloys is observed in [15].

Dark particles are present in the electron microscopic images shown in Fig. 7. This may be due to contamination of the material mainly by particles coming from metal oxides during sample preparation using jet-type electrical discharge equipment. Thus, in the work [23], a similar phenomenon was observed after milling the alloy of the CoCrFeNi system.

Changing the zirconium and manganese content has a significant effect on the nanohardness, microhardness, and Young's modulus of the CoCrZrMnNi alloys, which can lead to various structural transformations and mechanical characteristics. Thus, in the study [16], a similar effect was observed from varying the percentage content of Fe and Mn from 5 to 35 at. %, which led to a nonlinear change in the strength properties of these materials, which are decisive for the use of HEA in modern structural materials. The conducted studies confirm the assumption about the strengthening effect of HEA with an increased zirconium content.

CONCLUSIONS

It was found that the production of high-entropy alloys of the CoCrZrMnNi system by vacuum-induction melting contributes to the production of alloys with a heterogeneous structure and various mechanical properties:

1. An increase in the zirconium content in the CoCrZrMnNi alloys from 8 to 28 at. % contributed to the formation of a fine-grained structure and a more uniform elemental distribution.

2. The $Co_{19.8}Cr_{17.5}Zr_{15.3}Mn_{27.7}Ni_{19.7}$ alloy demonstrated the highest nanohardness (10 GPa) and Young's modulus (161 GPa) during instrumental indentation. At the same time, the $Co_{20.4}Cr_{18.0}Zr_{7.9}Mn_{33.3}Ni_{20.3}$ alloy has the lowest mechanical properties (nanohardness, Young's modulus, and microhardness) among other alloys, which may be due to the coarse-grained structure. As the indenter load increased (5 N), the microhardness of the $Co_{19.8}Cr_{17.5}Zr_{15.3}Mn_{27.7}Ni_{19.7}$ alloy decreased compared to the $Co_{18.7}Cr_{16.5}Zr_{28.9}Mn_{17.4}Ni_{18.6}$ alloy, which may indicate more universal mechanical properties of alloys with a zirconium content of 20 at. %.

REFERENCES

1. Pandey V., Seetharam R., Chelladurai H. A comprehensive review: Discussed the effect of high-entropy alloys as reinforcement on metal matrix composite properties, fabrication techniques, and applications. *Journal of Alloys and Compounds*, 2024, vol. 1002, article number 175095. DOI: 10.1016/j.jallcom.2024.175095.
2. Zosu S.J., Amaghionyeodiwe C.A., Adedeji K.A. Optimization of high-entropy alloys (HEAS) for lightweight automotive components: Design, fabrication, and performance enhancement. *Global Journal of Engineering and Technology Advances*, 2024, vol. 21, no. 1, pp. 064–072. DOI: 10.30574/gjeta.2024.21.1.0182.
3. Ahmadkhaniha D., Zanella C. High Entropy Alloy Deposition from an Aqueous Bath. *Meeting abstracts*, 2023, vol. MA2023-02, article number 1263. DOI: 10.1149/ma2023-02201263mtgabs.
4. Rogachev A.S. Structure, stability, and properties of high-entropy alloys. *Physics of Metals and Metallography*, 2020, vol. 121, no. 8, pp. 733–764. DOI: 10.1134/S0031918X20080098.
5. Kao Yih-Farn, Chen Ting-Jie, Chen Swe-Kai, Yeh Jien-Wei. Microstructure and mechanical property of as-cast, homogenized and deformed $Al_xCoCrFeNi$ ($0 \le x \le 2$) high-entropy alloys. *Journal of Alloys and Compounds*, 2009, vol. 488, pp. 57–64. DOI: 10.1016/j.jallcom.2009.08.090.
6. Poletti M.G., Fiore G., Gili F., Mangherini D., Battezzati L. Development of a new high entropy alloy for wear resistance: FeCoCrNiW0.3 and FeCoCrNiW0.3 + + 5 at.% of C. *Materials and Design*, 2017, vol. 115, pp. 247–254. DOI: 10.1016/j.matdes.2016.11.027.
7. Tabachnikova E.D., Podolskiy A.V., Laktionova M.O., Bereznaia N.A., Tikhonovsky M.A., Tortika A.S. Mechanical properties of the CoCrFeNiMnVx high entropy alloys in temperature range 4.2–300 K. *Journal of Alloys and Compounds*, 2017, vol. 698, pp. 501–509. DOI: 10.1016/j.jallcom.2016.12.154.
8. Gludovatz B., Hohenwarter A., Catoor D., Chang E.H., George E.P., Ritchie R.O. A fracture-resistant high entropy alloy for cryogenic applications. *Science*, 2014, vol. 345, pp. 1153–1158. DOI: 10.1126/science.1254581.
9. Kim Han-Eol, Kim Jae-Hyun, Jeong Ho-In, Cho Young-Tae, Salem O., Jung Dong-Won, Lee Choon-Man. Effects of Mo Addition on Microstructure and Corrosion Resistance of $Cr_{25-x}Co_{25}Ni_{25}Fe_{25}Mo_x$ High-Entropy Alloys via Directed Energy Deposition. *Micromachines*, 2024, vol. 15, no. 10, article number 1196. DOI: 10.3390/mi15101196.
10. Nesterov K.M., Farrakhov R.G., Aubakirova V.R., Islamgaliev R.K., Sirazeeva A.R., Abuayyash A. Thermal stability and corrosion resistance of ultrafine-grained high-entropy $Fe_{30}Ni_{30}Mn_{30}Cr_{10}$ alloy. *Frontier Materials & Technologies*, 2022, no. 4, pp. 81–89. DOI: 10.18323/2782-4039-2022-4-81-89.
11. Yeh Jien-Wei. Alloy Design Strategies and Future Trends in High-Entropy Alloys. *JOM*, 2013, vol. 65, pp. 1759–1771. DOI: 10.1007/s11837-013-0761-6.
12. Yong Zhang, Ting Ting Zuo, Zhi Tang, Michael C. Gao, Dahmen K.A., Liaw P.K., Zhao Ping Lu. Microstructures and properties of high-entropy alloys. *Progress in Materials Science*, 2014, vol. 61, pp. 1–93. DOI: 10.1016/j.pmatsci.2013.10.001.
13. Cantor B., Chang I.T.H., Knight P., Vincent A.J.B. Microstructural development in equiatomic multi-

component alloys. *Materials Science and Engineering: A*, 2004, vol. 375–377, pp. 213–218. DOI: 10.1016/j.msea.2003.10.257.
14. Gromov V.E., Konovalov S.V., Chen X., Efimov M.O., Panchenko I.A., Shlyarov V.V. Development vector for enhancement of Cantor HEA properties. *Bulletin of the Siberian State Industrial University*, 2023, no. 2, pp. 3–12. DOI: 10.57070/2304-4497-2023-2(44)-3-12.
15. Drobyshev V.K., Panchenko I.A., Konovalov S.V. Mechanical properties and microstructure of alloys of the CoCrFeMnNi system. *Polzunovskiy vestnik*, 2024, no. 2, pp. 249–254. DOI: 10.25712/ASTU.2072-8921.2024.02.033.
16. Panchenko I.A., Drobyshev V.K., Konovalov S.V., Bessonov D.A. Structural Change in Co–Cr–Fe–Mn–Ni Alloys upon Variation in Mn and Fe Concentrations. *Technical Physics Letters*, 2024, no. 7. DOI: 10.1134/S1063785024700391.
17. Huo Wenyi, Zhou Hui, Fang Feng, Xie Zonghan, Jiang Jianqing. Microstructure and mechanical properties of $CoCrFeNiZr_x$ eutectic high-entropy alloys. *Materials and Design*, 2017, vol. 134, pp. 226–233. DOI: 10.1016/j.matdes.2017.08.030.
18. Polunina A.O., Polunin A.V., Krishtal M.M. The influence of addition of ZrO_2 nanoparticles to the electrolyte on the structure and anticorrosion properties of oxide layers formed by plasma electrolytic oxidation on the $Mg_{97}Y_2Zn_1$ alloy. *Frontier Materials & Technologies*, 2023, no. 4, pp. 87–98. DOI: 10.18323/2782-4039-2023-4-66-8.
19. Xu Haijian, Lu Zheng, Wang Dongmei, Liu Chunming. Microstructure Refinement and Strengthening Mechanisms of a 9Cr Oxide Dispersion Strengthened Steel by Zirconium Addition. *Nuclear Engineering and Technology*, 2017, vol. 49, no. 1, pp. 178–188. DOI: 10.1016/j.net.2017.01.002.
20. He J.Y., Wang H., Huang H.L. et al. A precipitation-hardened high-entropy alloy with outstanding tensile properties. *Acta Materialia*, 2016, vol. 102, pp. 187–196. DOI: 10.1016/j.actamat.2015.08.076.
21. Otto F., Hanold N.L., George E.P. Microstructural evolution after thermomechanical processing in an equiatomic, single-phase CoCrFeMnNi high-entropy alloy with special focus on twin boundaries. *Intermetallics*, 2014, vol. 54, pp. 39–48. DOI: 10.1016/j.intermet.2014.05.014.
22. Campari E.G., Casagrande A., Colombini E., Gualtieri M.L., Veronesi P. The effect of Zr addition on melting temperature, microstructure, recrystallization and mechanical properties of a Cantor high entropy alloy. *Materials*, 2021, vol. 14, no. 20, article number 5994. DOI: 10.3390/ma14205994.
23. Moravcik I., Kubicek A., Moravcikova-Gouvea L., Ondrej A., Kana V., Pouchly V., Zadera A., Dlouhy I. The Origins of High-Entropy Alloy Contamination Induced by Mechanical Alloying and Sintering. *Metals*, 2020, vol. 10, no. 9, article number 1186. DOI: 10.3390/met10091186.

СПИСОК ЛИТЕРАТУРЫ

1. Pandey V., Seetharam R., Chelladurai H. A comprehensive review: Discussed the effect of high-entropy alloys as reinforcement on metal matrix composite properties, fabrication techniques, and applications // Journal of Alloys and Compounds. 2024. Vol. 1002. Article number 175095. DOI: 10.1016/j.jallcom.2024.175095.
2. Zosu S.J., Amaghionyeodiwe C.A., Adedeji K.A. Optimization of high-entropy alloys (HEAS) for lightweight automotive components: Design, fabrication, and performance enhancement // Global Journal of Engineering and Technology Advances. 2024. Vol. 21. № 1. P. 064–072. DOI: 10.30574/gjeta.2024.21.1.0182.
3. Ahmadkhaniha D., Zanella C. High Entropy Alloy Deposition from an Aqueous Bath // Meeting abstracts. 2023. Vol. MA2023-02. Article number 1263. DOI: 10.1149/ma2023-02201263mtgabs.
4. Rogachev A.S. Structure, stability, and properties of high-entropy alloys // Physics of Metals and Metallography. 2020. Vol. 121. № 8. P. 733–764. DOI: 10.1134/S0031918X20080098.
5. Kao Yih-Farn, Chen Ting-Jie, Chen Swe-Kai, Yeh Jien-Wei. Microstructure and mechanical property of as-cast, homogenized and deformed $Al_xCoCrFeNi$ ($0 \le x \le 2$) high-entropy alloys // Journal of Alloys and Compounds. 2009. Vol. 488. P. 57–64. DOI: 10.1016/j.jallcom.2009.08.090.
6. Poletti M.G., Fiore G., Gili F., Mangherini D., Battezzati L. Development of a new high entropy alloy for wear resistance: FeCoCrNiW0.3 and FeCoCrNiW0.3 + + 5 at. % of C // Materials and Design. 2017. Vol. 115. P. 247–254. DOI: 10.1016/j.matdes.2016.11.027.
7. Tabachnikova E.D., Podolskiy A.V., Laktionova M.O., Bereznaia N.A., Tikhonovsky M.A., Tortika A.S. Mechanical properties of the CoCrFeNiMnVx high entropy alloys in temperature range 4.2–300 K // Journal of Alloys and Compounds. 2017. Vol. 698. P. 501–509. DOI: 10.1016/j.jallcom.2016.12.154.
8. Gludovatz B., Hohenwarter A., Catoor D., Chang E.H., George E.P., Ritchie R.O. A fracture-resistant high entropy alloy for cryogenic applications // Science. 2014. Vol. 345. P. 1153–1158. DOI: 10.1126/science.1254581.
9. Kim Han-Eol, Kim Jae-Hyun, Jeong Ho-In, Cho Young-Tae, Salem O., Jung Dong-Won, Lee Choon-Man. Effects of Mo Addition on Microstructure and Corrosion Resistance of $Cr_{25-x}Co_{25}Ni_{25}Fe_{25}Mo_x$ High-Entropy Alloys via Directed Energy Deposition // Micromachines. 2024. Vol. 15. № 10. Article number 1196. DOI: 10.3390/mi15101196.
10. Нестеров К.М., Фаррахов Р.Г., Аубакирова В.Р., Исламгалиев Р.К., Сиразеева А.Р., Абуайяш А. Термическая стабильность и коррозионная стойкость ультрамелкозернистого высокоэнтропийного сплава $Fe_{30}Ni_{30}Mn_{30}Cr_{10}$ // Frontier Materials & Technologies. 2022. № 4. С. 81–89. DOI: 10.18323/2782-4039-2022-4-81-89.
11. Yeh Jien-Wei. Alloy Design Strategies and Future Trends in High-Entropy Alloys // JOM. 2013. Vol. 65. P. 1759–1771. DOI: 10.1007/s11837-013-0761-6.
12. Yong Zhang, Ting Ting Zuo, Zhi Tang, Michael C. Gao, Dahmen K.A., Liaw P.K., Zhao Ping Lu. Microstructures and properties of high-entropy alloys // Progress in Materials Science. 2014. Vol. 61. P. 1–93. DOI: 10.1016/j.pmatsci.2013.10.001.
13. Cantor B., Chang I.T.H., Knight P., Vincent A.J.B. Microstructural development in equiatomic multicomponent alloys // Materials Science and Engineering: A. 2004. Vol. 375–377. P. 213–218. DOI: 10.1016/j.msea.2003.10.257.

14. Громов В.Е., Коновалов С.В., Чен С., Ефимов М.О., Панченко И.А., Шляров В.В. Вектор развития улучшения свойств ВЭС Кантора // Вестник Сибирского государственного индустриального университета. 2023. № 2. С. 3–12. DOI: 10.57070/2304-4497-2023-2(44)-3-12.
15. Дробышев В.К., Панченко И.А., Коновалов С.В. Механические свойства и микроструктура сплавов системы CoCrFeMnNi // Ползуновский вестник. 2024. № 2. С. 249–254. DOI: 10.25712/ASTU.2072-8921.2024.02.033.
16. Panchenko I.A., Drobyshev V.K., Konovalov S.V., Bessonov D.A. Structural Change in Co–Cr–Fe–Mn–Ni Alloys upon Variation in Mn and Fe Concentrations // Technical Physics Letters. 2024. № 7. DOI: 10.1134/S1063785024700391.
17. Huo Wenyi, Zhou Hui, Fang Feng, Xie Zonghan, Jiang Jianqing. Microstructure and mechanical properties of $CoCrFeNiZr_x$ eutectic high-entropy alloys // Materials and Design. 2017. Vol. 134. P. 226–233. DOI: 10.1016/j.matdes.2017.08.030.
18. Полунина А.О., Полунин А.В., Криштал М.М. Влияние добавки наночастиц ZrO_2 в электролит на структуру и антикоррозионные свойства оксидных слоев, формируемых плазменно-электролитическим оксидированием на сплаве $Mg_{97}Y_2Zn_1$ // Frontier Materials & Technologies. 2023. № 4. С. 87–98. DOI: 10.18323/2782-4039-2023-4-66-8.
19. Xu Haijian, Lu Zheng, Wang Dongmei, Liu Chunming. Microstructure Refinement and Strengthening Mechanisms of a 9Cr Oxide Dispersion Strengthened Steel by Zirconium Addition // Nuclear Engineering and Technology. 2017. Vol. 49. № 1. P. 178–188. DOI: 10.1016/j.net.2017.01.002.
20. He J.Y., Wang H., Huang H.L. et al. A precipitation-hardened high-entropy alloy with outstanding tensile properties // Acta Materialia. 2016. Vol. 102. P. 187–196. DOI: 10.1016/j.actamat.2015.08.076.
21. Otto F., Hanold N.L., George E.P. Microstructural evolution after thermomechanical processing in an equiatomic, single-phase CoCrFeMnNi high-entropy alloy with special focus on twin boundaries // Intermetallics. 2014. Vol. 54. P. 39–48. DOI: 10.1016/j.intermet.2014.05.014.
22. Campari E.G., Casagrande A., Colombini E., Gualtieri M.L., Veronesi P. The effect of Zr addition on melting temperature, microstructure, recrystallization and mechanical properties of a Cantor high entropy alloy // Materials. 2021. Vol. 14. № 20. Article number 5994. DOI: 10.3390/ma14205994.
23. Moravcik I., Kubicek A., Moravcikova-Gouvea L., Ondrej A., Kana V., Pouchly V., Zadera A., Dlouhy I. The Origins of High-Entropy Alloy Contamination Induced by Mechanical Alloying and Sintering // Metals. 2020. Vol. 10. № 9. Article number 1186. DOI: 10.3390/met10091186.

Структура и механические свойства высокоэнтропийных сплавов системы CoCrZrMnNi, полученных вакуумно-индукционной плавкой, с разным содержанием Zr и Mn

Коновалов Сергей Валерьевич*[1,2,3], доктор технических наук, профессор,
проректор по научной и инновационной деятельности
Дробышев Владислав Константинович[1,4], аспирант кафедры обработки металлов давлением и материаловедения ЕВРАЗ ЗСМК, научный сотрудник лаборатории электронной микроскопии и обработки изображений
Панченко Ирина Алексеевна[1,5], кандидат технических наук, доцент кафедры менеджмента качества и инноваций, заведующий лабораторией электронной микроскопии и обработки изображений
Ли Хайсинь[2,6], кандидат наук, доцент Научно-исследовательского института в Яньтае
[1]*Сибирский государственный индустриальный университет, Новокузнецк (Россия)*
[2]*Харбинский инженерный университет, Яньтай (Китай)*

***E-mail:** konovalov@sibsiu.ru

[3]ORCID: https://orcid.org/0000-0003-4809-8660
[4]ORCID: https://orcid.org/0000-0002-1532-9226
[5]ORCID: https://orcid.org/0000-0002-1631-9644
[6]ORCID: https://orcid.org/0000-0002-3444-115X

Поступила в редакцию 29.11.2024 *Пересмотрена 30.01.2025* *Принята к публикации 19.02.2025*

Аннотация: Изучены механические свойства и микроструктура высокоэнтропийных сплавов (ВЭС) системы CoCrZrMnNi, полученных вакуумно-индукционной плавкой, в зависимости от изменения содержания Zr и Mn. Оценивается влияние процентного содержания Zr и Mn на микроструктуру и механические свойства (модуль Юнга, нанотвердость, микротвердость) ВЭС системы CoCrZrMnNi. Изучена связь варьирования процентного содержания Zr и Mn с изменением размера зерен и механических свойств ВЭС. Исследования структуры, химического состава и распределения интенсивности характеристического рентгеновского излучения атомов выполнены с использованием сканирующей электронной микроскопии. Методами сканирующей электронной микроскопии продемонстрировано, что в сплавах CoCrZrMnNi при увеличении содержания циркония и уменьшении содержания марганца ближе к эквиатомному составу структура материала становилась более однородной. Изменение процентного содержания циркония с 8 до 28 ат. % способствовало уменьшению зерна с 30 до 5 мкм и более однородному элементному распределению. Сплав $Co_{19,8}Cr_{17,5}Zr_{15,3}Mn_{27,7}Ni_{19,7}$ в ходе инструментального индентирования

с нагрузкой на индентор 50 мН продемонстрировал наибольшее значение нанотвердости (10 ГПа) и модуля Юнга (161 ГПа). Сплав $Co_{20,4}Cr_{18,0}Zr_{7,9}Mn_{33,3}Ni_{20,3}$ обладает наименьшими параметрами нанотвердости, модуля Юнга, микротвердости среди других сплавов, что может быть связано с крупнозернистой структурой с размером зерна до 30 мкм. По мере увеличения нагрузки на индентор до 5 Н микротвердость сплава $Co_{19,8}Cr_{17,5}Zr_{15,3}Mn_{27,7}Ni_{19,7}$ снижалась по сравнению со сплавом $Co_{18,7}Cr_{16,5}Zr_{28,9}Mn_{17,4}Ni_{18,6}$, что может указывать на более универсальные механические свойства сплавов с эквиатомным содержанием циркония.

Ключевые слова: структура; механические свойства; высокоэнтропийный сплав; вакуумная индукционная плавка; сканирующая электронная микроскопия; модуль Юнга; нанотвердость; микротвердость.

Благодарности: Исследование выполнено за счет гранта Российского научного фонда № 23-49-00015, https://rscf.ru/project/23-49-00015/.

Для цитирования: Коновалов С.В., Дробышев В.К., Панченко И.А., Ли Хайсинь. Структура и механические свойства высокоэнтропийных сплавов системы CoCrZrMnNi, полученных вакуумно-индукционной плавкой, с разным содержанием Zr и Mn // Frontier Materials & Technologies. 2025. № 1. С. 21–34. DOI: 10.18323/2782-4039-2025-1-71-2.